ARMA 20–2040

Laboratory modeling of induced microseismicity in the Illinois Basin

Makhnenko, R.Y., Bondarenko, N.B., and Kim, K.
Department of Civil and Environmental Engineering, University of Illinois at Urbana-Champaign, Urbana, IL, USA
Whittaker, S.
Prairie Research Institute, University of Illinois at Urbana-Champaign, Champaign, IL, USA

ABSTRACT: The CarbonSAFE Macon County Project is evaluating the potential for injecting and geologically storing commercial quantities of CO_2 captured from large industrial emitters in the Illinois Basin. Determining the potential for induced seismicity is an important component of this evaluation. Microseismic activity recorded from previous demonstration projects appears to be related to development on planes of weakness in the low-permeable Precambrian crystalline basement that lies below the injection formation. To evaluate induced seismicity risk for the development of large commercial projects, detailed investigations of fault stability should be performed case specifically before injection starts. In the case of Illinois Basin, industrial scale projects could potentially involve carbon dioxide injection of several million tonnes CO_2 per year, so both the geomechanical properties of rocks and fault material and the stress state should be properly characterized. In this study, the cores of Precambrian rhyolite are recovered from more than 2 km depth in CarbonSAFE Macon County Well and preliminary X-ray CT scanning shows presence of sealed fractures in some of them, while others appear to be intact. The influence of fractures on rock's poroelastic and strength properties is investigated. Laboratory data is used in a numerical code to simulate the reservoir and basement response and explain the observed induced seismicity.

1. INTRODUCTION

The CarbonSAFE Macon County project is evaluating the potential for injecting and geologically storing CO_2 captured from large industrial emitters in the Illinois Basin. A consideration of this evaluation is the potential to induce seismic activity as a result of increased reservoir pressures from commercial-scale injection. Induced seismicity is of a major concern, because it is believed that even small- to moderate-sized earthquakes threaten the seal integrity of CO_2 repositories, possessing significant risk on large scale storage operations (Zoback and Gorelick, 2012). A demonstration carbon capture and storage (CCS) project - the Illinois Basin Decatur Project (IBDP) injected approximately 1MT CO_2 over three years into a Cambrian sandstone reservoir about 2,100 m deep in the Illinois Basin (Bauer et al., 2016), underlain mainly by the Eastern Granit-Rhyolite province (Leetaru and Freiburg, 2014). Deep wellbore geophones at IBDP detected microseismic activity believed to be concentrated in the crystalline basement (Goertz-Allmann et al., 2017; Bauer et al., 2019) right below the injection formation. The basement has small porosity (<0.02) and permeability ($<10^{-19}$ m^2), therefore, it could be possible that reservoir overpressure transfers to the basement through preexisting fractures.

Basement fractures or faults elsewhere are seen up to 4-5 orders of magnitude more permeable than intact rock (Rutqvist, 2015). For CCS projects in general, it is important to understand the geomechanical behavior not just of the reservoir and seal, but also the underlying geologic units. Pressure perturbation can reach large distances through the reservoir and, if it intersects a fault in the crystalline basement, it will pressurize it. Even a distant fault that is large enough and oriented in a specific way could be reactivated (White and Foxall, 2016). The mobilized friction angle increases due to the rise of the pore fluid pressure, thus bringing the stress state closer to failure. The crystalline basements, in general, become critically stressed due to its high stiffness. The maximum frequency of tectonically induced earthquake swarms is observed at depths of 5-6 km, but it can be expected at much shallower depths where

effective minimum principle stresses are lower (Vilarrasa and Carrera, 2015). To evaluate induced seismicity risk, detailed geomechanical investigations of fault stability should be carried out case specifically before injection starts. In order to perform such analysis, both the geomechanical properties of rock and fault material and the stress state should be characterized (Vilarrasa *et al.*, 2019).

In this study, Precambrian rhyolite from the crystalline basement of the Illinois Basin is tested in two states: intact and fractured, to investigate the conditions at which a felt induced seismicity could occur in this formation. Laboratory tests are performed on core samples from McMillen #2, a well drilled in Christian County, IL for the CarbonSAFE project, and well VW#1 of the IBDP project. Each well penetrates the Precambrian basement. Elastic and inelastic material properties, as well as permeability, are dependent on depth and proper evaluation is needed for accurate interpretation of microseismic activity.

2. MATERIAL

This study utilizes two 88 mm in diameter and 250 mm long cores of Precambrian rhyolite coming from the CarbonSAFE well from depths of 1950 and 1970 meters. Energy Dispersive X-ray Spectroscopy analysis indicates that the intact rock is mainly made of silica, while the fracture surfaces contained significate fractions of potassium and calcium, as well as traces of titanium (Figure 1). The rhyolite from the IBDP well is reported to consist of quartz (31%), K-feldspar (12%), anorthite (12%), and more that 30% of clay minerals (Freiburg *et al.*, 2020).

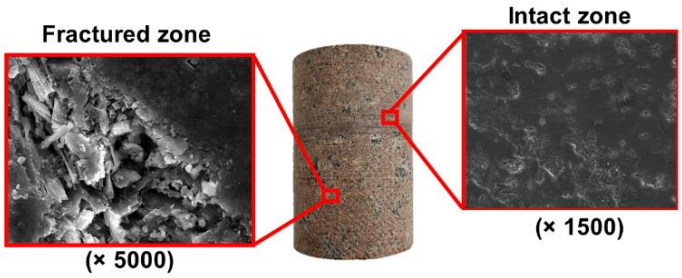

Fig. 1. Surface Electron Microscopy images indicating the differences in rock microstructure for intact and fractured material.

Dry density ρ is calculated as the mass of the cylindrical specimen divided by its volume and is reported to be 2.76 g/cm^3 for the intact rock, while for the fractured material it is 2.73 g/cm^3. The porosity ϕ is defined as the ratio between the interconnected pore space and the bulk volume. Interconnected porosity and pore size distribution of a tight rock can be accurately measured from porosimetry tests (Kuila and Prasad, 2013). The results of nitrogen adsorption test are presented in Figure 2 and indicate that pore widths of intact basement rock specimen span the range of 0.007 – 0.1 μm (micron) with the dominant pore size of 0.02 μm. The porosity of the basement rock is estimated to be $\phi = 0.01$.

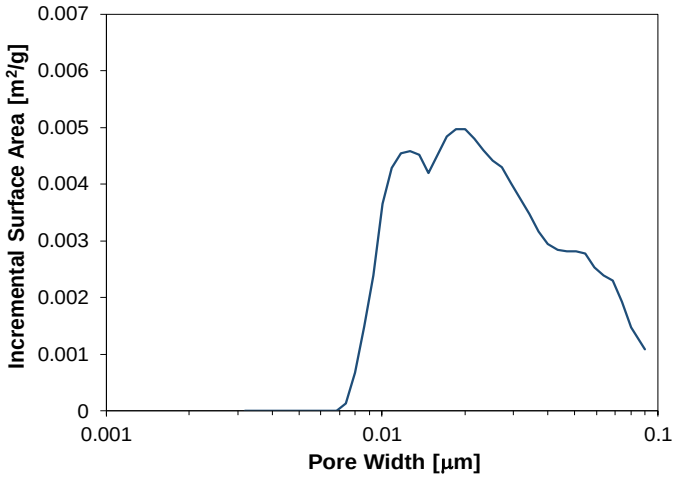

Fig. 2. Pore width distribution in intact basement rock specimen. The dominant pore width is 0.02 micron.

3. GEOMECHANICAL CHARACTERIZATION

3.1. Dynamic properties

Ultrasonic or "dynamic" elastic constants can be calculated from the measured wave velocities and the bulk density (Brown, 1981). With 2.25 MHz transducers (General Electric Alpha 2.25 MHz & Panametrics V154), both *P*- and *S*-waves (compressional and shear waves) are generated. The data acquisition system for the velocity measurements consists of an ultrasound pulse receiver, a digital oscilloscope, and sets of ultrasonic transducers. The through transmission measurements are repeated 128 times and time-averaged for improved signal-to-noise ratio (SNR). By visually and digitally examining the waveform, the departure time and arrival time can be determined for each wave type and *P*- and *S*-wave velocities, c_p and c_s, can be calculated. Given the material density ρ, the elastic parameters E – Young's modulus and ν – Poisson's ratio can be obtained using the following relationships

$$E = \frac{\rho c_s^{\,2}\left(3c_p^{\,2} - 4c_s^{\,2}\right)}{\left(c_p^{\,2} - c_s^{\,2}\right)} \quad (1)$$

$$\nu = \frac{c_p^{\,2} - 2c_s^{\,2}}{2\left(c_p^{\,2} - c_s^{\,2}\right)} \quad (2)$$

Seventeen rock specimens of irregular shape are tested for ultrasonic velocities and density. The rock comes from depths between 2149 m to 2154 m from VW1 well at IBDP and is recognized as Precambrian rhyolite. The dynamic Young's modulus is calculated to vary from 52 to 76 GPa, Poisson's ratio is 0.15-0.23, porosity is 0.0004-0.011, and density is 2.49-2.77 g/cm^3 (Figure 3). The parameters vary by up to 20% from one specimen to another without any clear dependence on the depth and the degree of 2D anisotropy is evaluated to be up to 7%.

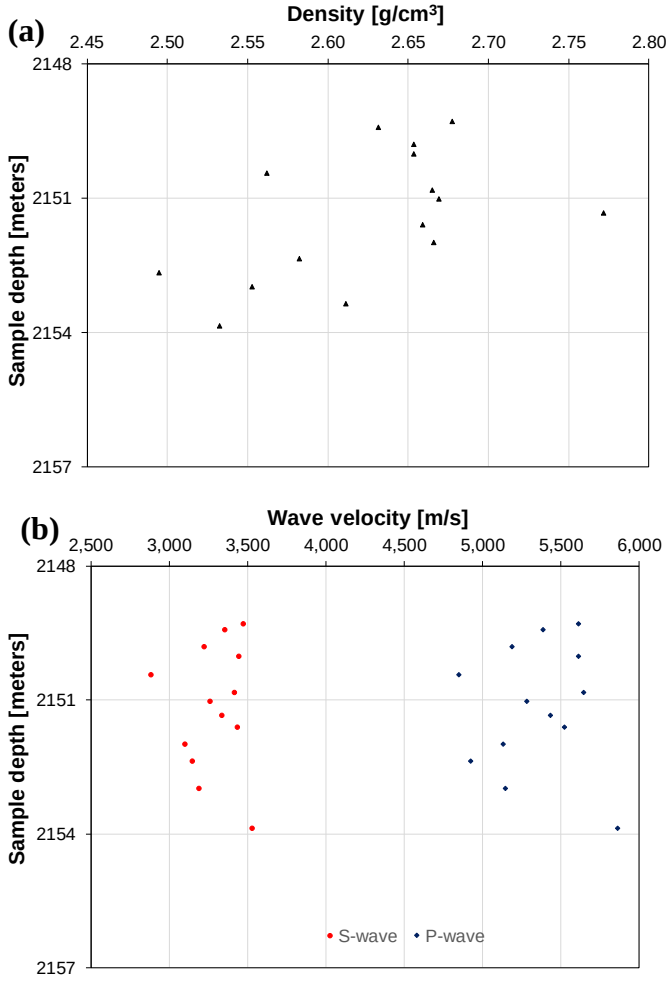

Fig. 3. (a) Density and (b) ultrasonic velocities of the basement rock from Illinois Basin as functions of the depth from the surface.

The ultrasonic velocities are also measured on intact and fractured samples from CarbonSAFE Macon well. *P*- and *S*-wave velocities (c_p [km/s], c_s [km/s]) are (5.33, 3.28) for the intact rock and (5.52, 3.16) for the fractured sample. This leads to E = 71 GPa and $\nu = 0.20$ for the intact material, while the fractured one appears to be slightly more compressible with E = 68 GPa and $\nu = 0.25$. The dynamic properties measured for the CarbonSAFE well correlate well with the observations from the VW1 well.

3.2. Poroelastic properties

The unjacketed bulk modulus is measured for intact Precambrian rhyolite in the hydrostatic compression test (Makhnenko and Labuz, 2016). A prismatic specimen 50x35x27 mm instrumented with strain rosettes in three perpendicular directions is submerged in the hydraulic oil, which allowed to saturate the rock at 50 MPa cell pressure. The specimen is slowly unloaded making sure pore pressure diffusion occurs at every 2-3 MPa step that takes 2-3 days. Measurements of corresponding normal strains result in calculation of the unjacketed bulk modulus K_s' = 43.2 GPa (Figure 4). Knowledge of K_s' along with the drained bulk modulus $K = E/3/(1\text{-}2\nu)$ = 41 GPa allows estimation of other poroelastic properties: Biot coefficient α, Skempton's B coefficient, and the undrained Poisson's ratio ν_u (Detournay and Cheng, 1993).

$$\alpha = 1 - K/K_s' \quad (3)$$

$$B = \frac{\alpha}{\alpha + \phi K\left(\frac{1}{K_f} - \frac{1}{K_s''}\right)} \quad (4)$$

$$\nu_u = \frac{3\nu + \alpha B(1-2\nu)}{3 - \alpha B(1-2\nu)} \quad (5)$$

The Skempton's B coefficient depends on the bulk modulus of the pore fluid K_f and is calculated assuming that the unjacketed bulk modulus is equal to unjacketed pore modulus: $K_s' = K_s''$.

Intact basement rock has extremely low permeability that resulted in pore pressure dissipation time $t \approx 40$ hours in unjacketed prismatic specimens with the characteristic length l = 27 mm. The hydraulic diffusivity $c \sim l^2/4t$ can then be estimated for double drainage boundary condition and is used to calculate rock's permeability k

$$k \approx c\mu\phi\left(\frac{1}{K_f}+\frac{\alpha}{\phi K}\right) \quad (6)$$

Here μ is the dynamic viscosity of the fluid (μ_{oil} = 0.07 Pa·s) and the bulk modulus for pore fluid is taken as the one for hydraulic oil: K_{oil} = 1.3 GPa. This results in the estimated sub nano Darcy value of permeability $k = 0.7 \cdot 10^{-21}$ m^2.

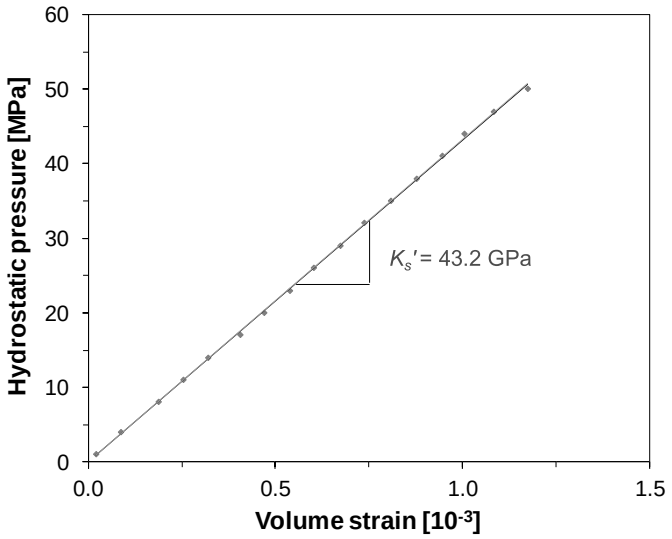

Fig. 4. Pressure – volume strain diagram for the unloading stage of the unjacketed hydrostatic compression test performed on intact basement rock.

3.3. Triaxial compression tests

The triaxial compression test is one of the most common experimental techniques deployed in the evaluation of strength and elastic properties of rock (Jaeger *et al.*, 2007). Triaxial tests are conducted in a Hoek-Franklin cell, with core diameters of 30.5 mm and lengths of 65-75 mm that are put inside rubber membranes and subjected to confining pressures of σ_3 = 10 and 20 MPa.

Specimens are cored in the horizontal direction, such that axial loading in conventional triaxial compression experiments are aligned with the direction of the maximum in-situ principal stress (Bauer *et al.*, 2019). The coring is performed through the rock that considered to be intact, as well as through the material that has visible but sealed fractures. After that, the specimens are ground flat within a tolerance of 0.05 mm using a surface grinder. All the attempts to core through the material with apparent fracture surfaces lead to the samples' failure through the planes of weakness. Total three intact specimens are prepared from the core that appeared to contain no fractures.

The specimen ends are lubricated with stearic acid mixture to promote homogeneous deformation (Labuz and Bridell, 1993) and the cell is installed inside 1 MN MTS load frame. Specimen are loaded with a displacement rate of 1×10^{-4} mm/s to ensure quasi-static deformation and axial load and axial specimen deformation are recorded and allowed reporting stress-strain diagrams for the tested rock (Brown, 1981). Figure 4 illustrates the results of two triaxial tests and one uniaxial compression test performed on a cylindrical specimen with the diameter of 36 mm and length of 70 mm. The response of the material is non-linear at the early stages of loading, which can be attributed to the closure of cracks. When deviatoric stress increases – the stress-strain curve appears to have a linear part and the accurate calibration of the system deformation allowed determination of the Young's modulus of the rock. It appeared to increase with the confining pressure from 52 GPa at 0 MPa to 69 GPa at 20 MPa, which can be explained by the closure of cracks in the rock at higher pressures. The basement rock response is brittle (typical for granitoids) and the material strength increases with the confining pressure (Figure 5).

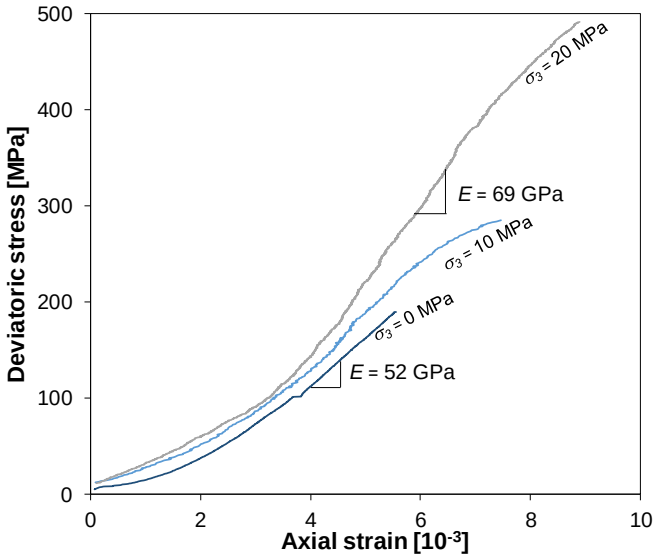

Fig. 5. Deviatoric stress - axial strain diagram for triaxial compression tests performed on intact basement rock specimens at 0, 10, and 20 MPa confining pressures.

The Young's modulus E and Poisson's ratio ν are also determined in uniaxial compression test using resistive strain gages. The material strength is determined to be 189 MPa with axial splitting being the failure mode. The measured Young's modulus E = 52 GPa and Poisson's ratio $\nu = 0.22$.

The results of the three tests are interpreted within the framework of a Mohr-Coulomb failure criterion (Labuz and Zang, 2012), where shear stress acting on the failure plane τ is linearly dependent on the effective normal stress σ_n':

$$\tau = c + \sigma_n' \cdot \tan(\varphi) \quad (7)$$

The best fit line in the shear stress - normal stress plane is associated with an angle of internal friction ϕ = 42° and an inherent shear strength (cohesion) c = 9.4 MPa (Figure 6). It appeared that all the specimens fail through pre-existing weak planes that are not visible during the specimen preparation. Such a low cohesion reported for granitic rock also indicates the influence of weak planes on the material strength. In addition to that, it can be assumed that cohesion of the specimens with visible weak planes is close to zero, since they failed easily during the coring. Investigation on whether the friction of the fractured rock could be assumed equal to the one of the material that appeared to be intact is still ongoing. Direct shear test with normal stress applied perpendicular to the fracture surface are often utilized to characterize the response of fractured rock (Jaeger *et al.*, 2007; Samuelson *et al.*, 2009). However, proper utilization of this test for the cores of Precambrian rhyolite would be very difficult, because the rock has number of non-planar and sometimes invisible fractures.

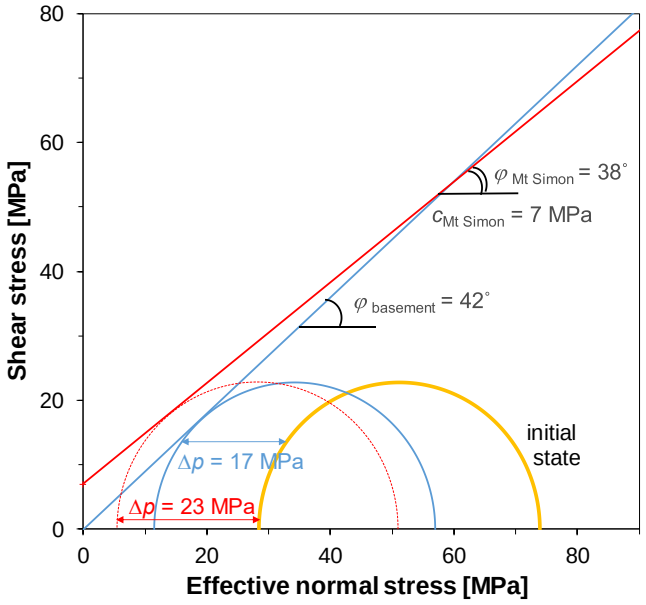

Fig. 6. Mohr-Coulomb failure envelope constructed for the basement rock assuming zero cohesion on preexisting weak planes and Mohr's circles representing state of stress at the top of the basement rock layer in Illinois Basin for different injection pressures.

4. IMPLICATIONS TO INDUCED SEISMICITY

In this section, the CO_2 injection in Illinois Basin in the interval between 2110 and 2120 m depth, approximately 20 meters above the Precambrian basement, is simulated (Figure 7). The maximum principal stress at the injection site is horizontal $\sigma_H = \sigma_1$ = 97 MPa. The vertical stress is the minor principal stress $\sigma_V = \sigma_3$ = 50 MPa, while the pore pressure p = 21.8 MPa – just slightly above the hydrostatic value (Bauer *et al.*, 2016). The Mohr's circle corresponding to the original state of stress at the injection well in IBDP is shown in orange in Figure 6. The necessary change of pore pressure to cause failure of the basement rock is Δp = 17 MPa assuming that the failure occurs through a cohesionless joint that has the same friction angle as the tested specimens (blue line and blue circle in Figure 6). Strength parameters for lower Mt Simon sandstone are taken as $\varphi = 38°$ and c = 7 MPa (Bauer *et al.*, 2016) and the he necessary change of pore pressure for failure is calculated to be Δp = 23 MPa (red line and red circle in Figure 6). This pressure is much above the maximum increase in the pore pressure (around 1.2 MPa) recorded in the reservoir during the injection phase in IBDP (Bauer *et al.*, 2016).

For evaluating CO_2 storage in the Illinois Basin, it is of interest to study possible changes of the pore pressure in the reservoir and surrounding rock. The constitutive model should include the poroelastic effect, the effects pore pressure concentration during injection, and multilayered injection site structure with different properties for each formation. In this study, we adopt the diffusion equation for the pore pressure p under irrotational displacement condition (Rudnicki, 1986; Detournay and Cheng, 1993).

$$\frac{\partial p}{\partial t} - c\nabla^2 p = \frac{\gamma}{S} \quad (8)$$

Here γ is the source density (the rate of injected fluid volume per unit volume of the porous solid) and S is the storage coefficient that can be calculated from

$$S = \frac{\alpha^2 (1-\nu_u)(1+\nu)(1-2\nu)^2}{E(1-\nu)(\nu_u - \nu)} \quad (9)$$

Knowing the injection rate q [kg/s], mass density of fluid in unstressed state ρ_f, and volume of the

injection zone V, the source density can be calculated as

$$\gamma = q / (V \rho_f) \quad (10)$$

Mass injection rate for the first stage of the IBDP is approximately 0.33 Mt/year, so the volume injection rate is $q/\rho_f = 0.01$ m^3/s. The injection zone is considered to be a parallelepiped with height of 9 m and 2 m side, so $V = 36$ m^3.

Idealized structure of the formations in the Illinois Basin is shown in Figure 7a. Properties of Precambrian basement are adopted from this study and the properties for lower Mt Simon and Argenta are taken from the logging and laboratory data (Freiburg *et al.*, 2016; Bauer *et al.*, 2016). Poroelastic parameters have not been reported for the involved formations, thus undrained Poisson's ratio and Biot coefficient are estimated based on our knowledge of the typical values for similar rock types (Detournay and Cheng, 1993; Makhnenko and Podladchikov, 2018). Since only permeability is available for the mudstone interlayer, its other properties are assumed to be those of the typical claystone (Makhnenko and Podladchikov, 2018). All this information is listed in Table 1.

For Lower Mt Simon sandstone, the source density is calculated to be $\gamma \approx 24$/day and the storage coefficient $S \approx 3 \cdot 10^{-10}$ 1/Pa. Viscosity of brine at the reservoir temperature of 70°C is $\mu = 4 \cdot 10^{-4}$ Pa·s and the mass density of the injection fluid (supercritical CO_2) at the same conditions is $\rho_f = 800$ kg/m^3 (Spycher *et al.*, 2003).

During CO_2 injection, we assume that the main pressure disturbance in the Illinois Basin away from the injection well and in the basement will be due to the flow of in-situ brine, rather than a free phase of CO_2, so we are considering a problem of pressure diffusion in aqueous fluid.

Distribution of pore pressure change is calculated by solving equation (8) with the parameters described above using PDE toolbox in Matlab©. Prediction for the pore pressure distribution after 1000 days of injection is shown in Figure 7b. The maximum overpressure predicted by the model is around 7 MPa and is achieved near the injection well and right underneath it in low-permeable Argenta layer. Comparing to the case of Illinois Basin Decatur Project, where the field observations reported not more than 1.2 MPa pore pressure increase (Bauer *et al.*, 2016), our prediction is an overestimation.

In addition to the case of the intact rock, another case with 1 m thick vertical fault with permeability two orders of magnitude higher than the surrounding media is considered (Figure 7a). In this case, the overpressure can travel through the Argenta layer to the Precambrian rhyolite and the maximum value it could reach on the basement fault is calculated to be 5.4 MPa (Figure 7c).

It should be noted that the model calculations are sensitive to the permeability and poroelastic properties (especially, the difference between drained and undrained Poisson's ratios) of the involved formations. Heterogeneities in the participating rock, as well as relatively high permeable faults, can play a significant role in pore pressure dissipation (Segall and Lu, 2015). Even if locally the pore pressure dissipation is inhibited (undrained condition), the deformation of the rock could be inelastic and generate significant microseismicity (Makhnenko and Labuz, 2015).

Table 1. Index properties, poroelastic parameters, permeability, and friction angle of the formations associated with Illinois Basin

Formation	Depth [m]	Porosity ϕ [–]	Young's Modulus E [GPa]	Drained Poisson's ratio ν [-]	Undrained Poisson's ratio ν_u [-]	Biot coefficient α [-]	Hydraulic diffusivity c [m^2/s]	Kinematic permeability k [m^2]	Friction angle φ [°]
Mudstone interlayer	2065 - 2070	0.12	2.8	0.33	0.40	0.75	$1.1*10^{-4}$	$1*10^{-18}$	24
Lower Mt Simon	2070 - 2120	0.19	16	0.21	0.25	0.70	3.1	$2*10^{-13}$	37
Argenta	2120 - 2140	0.07	50.0	0.25	0.30	0.31	$2.6*10^{-2}$	$3*10^{-16}$	38
Precambrian Basement	2140 and below	0.01	69	0.22	0.222	0.051	$1.2*10^{-9}$	$0.7*10^{-21}$	42

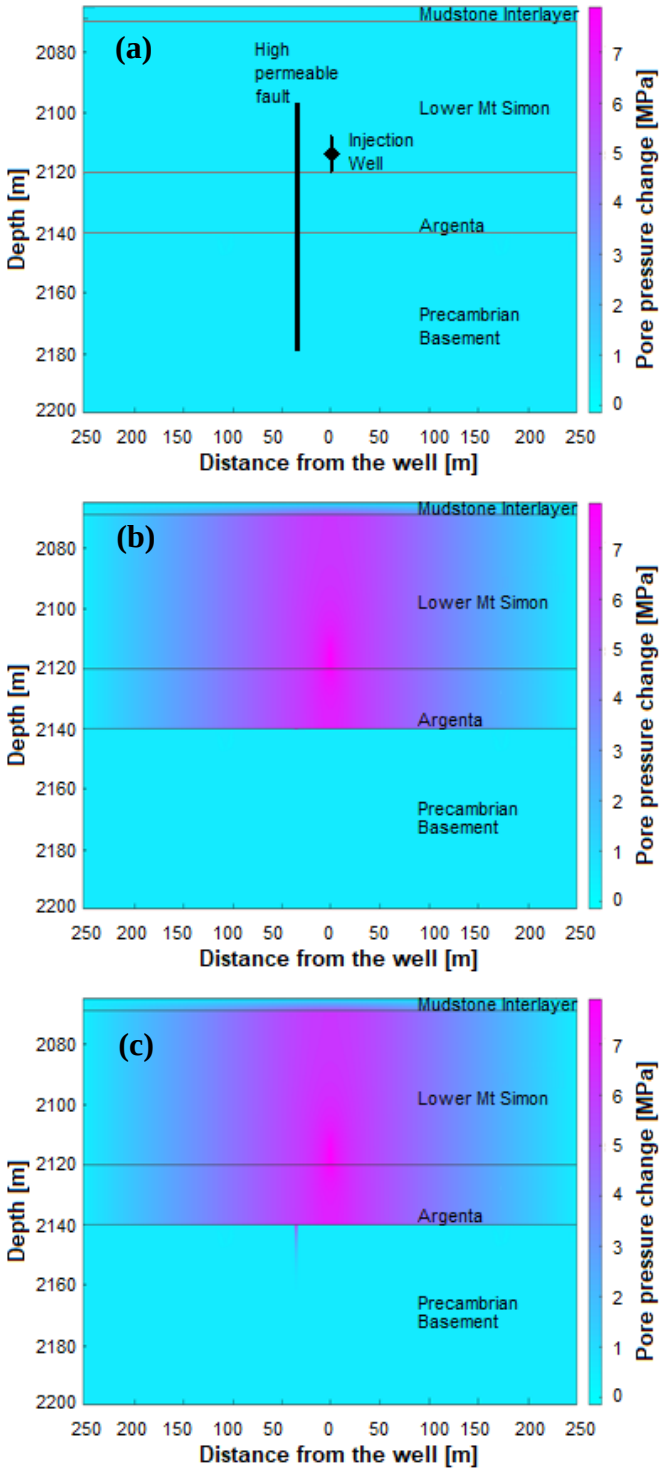

Fig 7. (a) Layout of the Illinois Basin rock formations near CarbonSAFE Macon County, initial overpressure (pore pressure change) is zero. (b) Overpressure after 1000 days of injection with volume rate of 0.01 [m^3/sec] without considering high permeable faults in the model. (c) Overpressure after 1000 days of injection with volume rate of 0.01 m^3/sec with high permeable fault (with permeability 100 times higher than that of the surrounding layer and width of 1 m). The properties of the layers are taken from this study, Freiburg *et al.* (2016), and Bauer *et al.* (2016).

The in-situ stress state in Central Illinois indicates that two horizontal stresses act as the major and intermediate principal stresses (Bauer *et al.*, 2016). The assessment of basement rock failure should consider both the directional dependency of strength properties and possible intermediate stress effect (Labuz *et al.*, 2018). Moreover, coupled thermo-hydro-mechanical (THM) effect of colder fluid injection and the potential chemical effect of the acidic mixture of CO_2 and brine could also have impact on the involved rock layers (Vilarrasa *et al.*, 2019). However, it is not expected that all the aforementioned factors combined could lead to 17 MPa increase in the pore pressure needed for intact rock failure. We believe that the main focus should be on addressing the properties of the fractured rock that locally could be significantly weaker than the intact material and provide pathways for fluid flow. Ideally, the constitutive model describing the injection site behavior should include proper loading conditions, all major rock formations and non-uniformities, accurately measured flow and mechanical properties for intact rock, fractured material, and fractures, as well as the coupled THM effect on the deformation and stress state.

5. CONCLUSIONS

Induced seismicity associated with CO_2 injection in deep Cambrian sandstones in the Illinois Basin is expected to be mainly associated with the fault activation in the basement rock. Intact and fractured cores of the Precambrian basement coming from more than 2 km depth are characterized for their elastic and strength properties. It appears that the conventional approach to addressing the induced seismicity would involve very high overpressures to be achieved in the jointed basement rock. However, the coupled effects of fluid injection, pore pressure diffusion, and thermal stress change also play the role and need to be addressed. The ongoing series of experiments include accurate measurements of basement rock poromechanical properties and permeability. We believe that the aforementioned tests will help to relieve the differences between the intact and fractured specimens of the basement rock from CarbonSAFE Macon County well. Laboratory data will be used in numerical codes to simulate the reservoir and basement response. Potentially, the observed induced seismicity will be explained and recommendations for the future projects will be made.

ACKNOWLEDGEMENTS

The authors acknowledge the support from US DOE through CarbonSAFE Macon County Project DE-FE0029381.

REFERENCES

Brown, E.T. 1981. *Rock Characterization, Testing and Monitoring: ISRM Suggested Methods.* International Society for Rock Mechanics: Oxford, Pergamon Press.

Bauer, R.A., M. Carney, and R.J. Finley. 2016. Overview of microseismic response to CO_2 injection into the Mt Simon saline reservoir at the Illinois Basin-Decatur project. *Int. J. Greenhouse Gas Control,* 54(1), 378-388.

Bauer, R.A., R. Will, S. Greenberg, and S.G. Whittaker. 2019. Illinois Basin-Decatur project. In *Geophysics and Geosequestration*, eds. T.M. Davis, M. Landrø, and M. Wilson, 339-369.

Detournay, E. and A.H.-D. Cheng. 1993. Fundamentals of Poroelasticity. In *Comprehensive rock engineering*, ed. C. Fairhurst, 114–168.

Freiburg, J.T., R.W. Ritzi, and K.S. Kehoe. 2016. Depositional and diagenetic controls on anomalously high porosity within a deeply buried CO_2 storage reservoir - the Cambrian Mt. Simon Sandstone, Illinois Basin, USA. *Int. J. Greenhouse Gas Control*, 55, 42–54.

Freiburg, J.T., J.H. McBride, D.H. Malone, and H.E. Leetaru. 2020. Petrology, geochronology, and geophysical characterization of Mesoproterozoic rocks in central Illinois, USA. *Geoscience Frontiers*, 11(2), 581-596.

Goertz-Allmann, B.P., S.J. Gibbons, V. Oye, R. Bauer, and R. Will. 2017. Characterization of induced seismicity patterns derived from internal structure in event clusters. *J. Geophys. Res. Solid Earth*, 122, 3875–3894.

Jaeger, J.C., N.G.W. Cook, and R.W. Zimmerman. 2007. *Fundamentals of Rock Mechanics.* 4th edition: Malden, MA, Blackwell.

Kuila, U., and M. Prasad. 2013. Specific surface area and pore-size distribution in clays and shales. *Geophys. Prospect.*, 61(2), 341-362.

Labuz, J.F. and J.M. Bridell. 1993. Reducing frictional constraint in compression testing through lubrication. *Int. J. Rock Mech. Mining Sci. & Geomech. Abs.*, 30(4), 451–455.

Labuz, J.F. and A. Zhang. 2012. Mohr-Coulomb failure criterion. *Rock Mech. Rock Eng.*, 45(6), 975–979.

Labuz, J.F, F. Zeng, R. Makhnenko, Y. Li. 2018. Brittle failure of rock: a review and general linear criterion. *J. Struct. Geol.*, 112, 7–28.

Leetaru, H.E. and J.T. Freiburg. 2014. Litho-facies and reservoir characterization of the Mt Simon Sandstone at the Illinois Basin-Decatur Project. *Greenhouse Gases: Sci. & Techn.*, 4 (5), 580–595.

Makhnenko, R. and J. Labuz. 2015. Dilatant hardening of fluid-saturated sandstone. *J. Geophys. Res. Solid Earth*, 120, 909-922.

Makhnenko, R. and J. Labuz. 2016. Elastic and inelastic deformation of fluid-saturated rock. *Philos. Trans. Royal Society A*, 374, 20150422.

Makhnenko, R.Y. and Y.Y. Podladchikov. 2018. Experimental poroviscoelasticity of common sedimentary rocks. *J. Geophys. Res. Solid Earth*, 123(9), 7586–7603.

Rudnicki, J.W. 1986. Fluid mass sources and point forces in linear elastic diffusive solids. *Mech Mater.*, 5(4), 383–393.

Rutqvist, J., 2015. Fractured rock stress-permeability relationships from in situ data and effects of temperature and chemical-mechanical couplings. *Geofluids*, 15(1-2), 48-66.

Samuelson, J., D. Elsworth, and C. Marone. 2009. Shear-induced dilatancy of fluid-saturated faults: Experiment and theory. *Journal of Geophysical Research*, 114, B12404.

Segall, P. and S. Lu. 2015. Injection-induced seismicity: Poroelastic and earthquake nucleation effects, *J. Geophys. Res. Solid Earth*, 120, 5082–5103.

Spycher, N., K. Pruess, and J. Ennis-King. 2003. CO2-H2O mixtures in the geological sequestration of CO2. I. Assessment and calculation of mutual solubilities from 12 to 100°C and up to 600 bar. *Geochim. Cosmochim. Acta*, 67, 3015–3031.

Vilarrasa, V., and J. Carrera. 2015. Geologic carbon storage is unlikely to trigger large earthquakes and reactivate faults through which CO_2 could leak. *Proc. Ntnl. Acad. Sci. USA*, 112, 5938–5943.

Vilarrasa, V., Makhnenko, R.Y., and Rutqvist, J., 2019. Field and laboratory studies of geomechanical response to the injection of CO_2. In *Science of Carbon Storage in Deep Saline Formations: Process Coupling Across Time and Spatial Scales*, eds. P. Newell and A. Ilgen, 159-178.

White, J.A. and W. Foxall. 2016. Assessing induced seismicity risk at CO_2 storage projects: Recent progress and remaining challenges. *Int. J. Greenhouse Gas Control*, 49, 413-434.

Zoback, M.D. and S.M. Gorelick. 2012. Earthquake triggering and large-scale geologic storage of carbon dioxide. *Proc. Ntnl. Acad. Sci. USA*, 109(26): 10164e8.